Chinese Chemical Letters 35 (2024) 109642

Contents lists available at ScienceDirect

Chinese Chemical Letters

journal homepage: www.elsevier.com/locate/cclet

Designed assembly of heterometallic cluster organic frameworks based on Th_6 cluster

Xianghe Kong[a,b], Xiaoli Liao[a], Zhenkun Huang[a], Lei Mei[b], Hongqing Wang[a], Kongqiu Hu[b,*], Weiqun Shi[b,*]

[a] School of Chemistry and Chemical Engineering, University of South China, Hengyang 421001, China
[b] Laboratory of Nuclear Energy Chemistry, Institute of High Energy Physics, Chinese Academy of Sciences, Beijing 100049, China

ARTICLE INFO

Article history:
Received 18 December 2023
Revised 26 January 2024
Accepted 4 February 2024
Available online 13 February 2024

Keywords:
Actinide
Hexanuclear thorium cluster
Heterometallic organic frameworks
Coordination chemistry
Catalytic cycloaddition

ABSTRACT

Four novel compounds based on hexanuclear thorium cluster were synthesized and characterized. Compound **1** [$Th_6(HPyC)_8(HCOO)_4$] is formed by replacing formate ligands of preassembled thorium cluster [$Th_6O_4(OH)_4(H_2O)_6(HCOO)_{12}$] with eight H_2PyC (4-pyrazolecarboxylic acid) under solvothermal conditions. Each of the $HPyC^-$ ligands is coordinated with one Cu^{2+} to form the (4,8)-connected ***scu***-net structure of compound **2** [$(CuCl_2)_2Th_6(HPyC)_8(HCOO)_4$]. In compound **3** [$(CuCl_2)_2Th_6(HPyC)_{10}(HCOO)_4$], ten of the formate ligands of preassembled Th_6 cluster are replaced by $HPyC^-$ ligands. Compared with compound **2**, the two extra $HPyC^-$ ligands in the equatorial plane of the Th_6 cluster in compound **3** are not further connected to copper ions. Therefore, the topology structure of compound **3** is same with that of compound **2**. Compound **4** [$(Cu_3Cl_2)(CuCl_2)Th_6(PyC)_3(HPyC)_4(HCOO)_5$] contains three kinds of metal nodes, Th_6 cluster, Cu_3 cluster and mononuclear Cu^{2+}, and exhibits a novel (5,7)-connected net structure, which was first discovered in actinide MOFs. Furthermore, considering the satisfactory stability of compound **4** and its unsaturated metal nodes and Lewis acid sites, the catalysis of cycloaddition of CO_2 was further studied. We found that this thorium-copper heterometallic cluster organic framework can be used as a potential actinide functional material for catalyzing the efficient CO_2 conversion to value-added products.

Thorium Molten Salt Reactor Nuclear Energy System (TMSR), as the fourth-generation reactor technology, has become the current international advanced nuclear energy research and development hotspot due to its outstanding safety and sustainable development [1–3]. The reserves of thorium in the Earth's crust is much higher than uranium, and thorium-based fuels have a higher energy output per unit weight and less waste generation compared to uranium [4–7]. Exploring novel thorium-based compounds is of great significance as it can provide valuable coordination chemistry information of thorium, which contributes to a comprehensive understanding of the chemical and physical properties of thorium under different conditions [8–10]. Th^{4+} cation has a larger ionic radius and coordination number than other tetravalent cations like Zr^{4+} and Hf^{4+}, making it easier to form metal nodes with richer coordination geometry [11–13]. In addition, Th^{4+} cations trend to hydrolysis in aqueous solution, resulting in cluster structures bridged by OH^-/O^{2-} groups [14–17]. With the in-depth understanding of thorium and the development of actinide metal functional materials, more and more thorium clusters and derived materials are synthesized and used in adsorption separation [18–20], catalysis [21,22], photo-sensing [23,24], radiation detection [25,26] and other fields.

In contrast to simple molecular thorium complexes or discrete thorium clusters, the assembly of thorium clusters with polycarboxylic acid ligands can produce thorium cluster organic frameworks (ThCOFs), which have excellent chemical and radiation stability and can serve as a unique platform for multifunctional applications [27]. For example, Volkringer *et al.* firstly synthesized a ThCOF $Th_6O_4(OH)_4(H_2O)_6(bdc)_6{\cdot}6DMF{\cdot}12H_2O$ with terephthalic acid by controlling the hydrolysis of Th^{4+} cations, which adopts the UiO-66 topology and exhibits a very high porosity [28]. Compared with Zr^{4+} and Hf^{4+} cations tending to adopt the eight-coordinate square antiprismatic geometry and forming $M_6(\mu_3\text{-}O)_4(\mu_3\text{-}OH)_4$ SBUs [29–31], Th^{4+} cations in the Th_6 clusters adopt a structure of nine-coordinate capped square antiprism geometry. The higher coordination number of Th^{4+} cations also opens up more possi-

* Corresponding authors.
E-mail addresses: hukq@ihep.ac.cn (K. Hu), shiwq@ihep.ac.cn (W. Shi).

https://doi.org/10.1016/j.cclet.2024.109642
1001-8417/

bilities for creating new and unique topologies. Recently, Lin *et al.* constructed a series of ThCOF materials (Th-SINAP) for iodine adsorption [32], ion recognition [33] and radiation detection [34] by the assembly of Th_6 clusters and polycarboxylic acid ligands, indicating the great potential application of thorium-based materials in the nuclear industry.

Heterometallic multi-component MOFs constructed based on clusters are gaining increasing attention due to their richer structural diversity and multifunctionality compared to the single-component MOFs [35–37]. A reasonable method for the synthesis of heterometallic MOFs is employing polyfunctional hybrid ligands or mixed ligands with varied coordination capabilities instead of polycarboxylic acid ligands, which is also suitable for the constructing of heterometallic ThCOFs. For example, Luo *et al.* used a multifunctional imidazole acid derivative ligand to combine 5f and 3d metal to obtain a $[Th_8Co_8]$ nanocage MOF with double screening ability, which can be used for clear separations of both H_2/D_2 isotopes and butane/or hexane isomers [38]. Hu and coauthors reported a viologen-based radical-containing heteroaromatic MOF with an unprecedented (6, 18)-connected ***she-d*** topology. This multicomponent MOF exhibits excellent visible/NIR light-driven CO_2 photoreduction activity [39].

Controlling polymorphic formation with identical precursors remains a challenging task in the construction of heterometallic ThCOFs due to the generation of different clusters during Th^{4+} hydrolysis [32,40]. Thus, it is urgent to develop a synthetic strategy to precisely control thorium clusters as a secondary building unit to assemble and construct new ThCOFs. In this work, a preassembled thorium cluster $[Th_6O_4(OH)_4(H_2O)_6(HCOO)_{12}]$ (abbreviated as Th_6) and a multifunction ligand 4-pyrazolecarboxylic acid (H_2PyC) are used to construct heterometallic ThCOFs. Through the regulation of experimental conditions, the H_2PyC ligand was exchanged with formate ligand on the Th_6 cluster to form the intermediate clusters $[Th_6O_4(OH)_4(H_2O)_6(HPyC)_x(HCOO)_{12-x}]$, which are further assembled with copper ions to form two kinds of thorium-copper heterometallic ThCOFs with different topologies. The reversibility of ligand exchange and the introduction of heterometallic copper ions enrich the structural diversity of thorium-based MOFs. More importantly, a thorium-copper heterometallic ThCOF has polymetallic active sites and Lewis acidity, making it a promising catalyst for CO_2 conversion.

$Th_6(\mu_3\text{-}O)_4(\mu_3\text{-}OH)_4(H_2O)_6(HPyC)_8(HCOO)_4{\cdot}4H_2O$ (**1**). Single-crystal X-ray structural determination shows that compound **1** crystallizes in a cubic space group *Immm* (Table S1 in Supporting information). As shown in Fig. 1a, the asymmetric unit contains two Th^{4+} cations with position occupancies of 0.5 (Th2) and 0.25 (Th1), respectively. Then two Th1 atoms and four Th2 atoms are bridged together by four μ_3-O and four μ_3-OH to form a typical $[Th_6(\mu_3\text{-}O)_4(\mu_3\text{-}OH)_4]^{12+}$ cluster, which is further coordinated by eight $HPyC^-$ ligands, four $HCOO^-$ ligands and six H_2O to form the final structure of compound **1**, as depicted in Fig. 1b. The Th_6 cluster is linked to two neighbouring units *via* multiple hydrogen bonds to form a 1D supramolecular chain (Fig. 1d). Adjacent 1D supramolecular chains are connected to one another by a series of lattice H_2O molecules *via* multiple hydrogen bonds (Fig. 1c), resulting in a 3D porous structure (Fig. 1e).

$(CuCl_2)_2Th_6(\mu_3\text{-}O)_4(\mu_3\text{-}OH)_4(HPyC)_8(HCOO)_4(H_2O)_6$ (**2**). Compound **2** crystallizes in an orthorhombic space group *Pbam* (Table S1). The asymmetric unit of compound **2** consists of 1/4 $Th_6(\mu_3\text{-}O)_4(\mu_3\text{-}OH)_4(H_2O)_6$ cluster, 1/2 $CuCl_2$ unit, two crystallographically independent $HPyC^-$ ligands and two $HCOO^-$ ligands with position occupancy of 0.5, as shown in Fig. 2a. Each Th_6 cluster is surrounded by four $HCOO^-$ ligands and eight $HPyC^-$ ligands, and further connected with eight Cu atoms (Fig. 2b). As shown in Fig. 2c, the Cu atom has an elongated octahedral configuration with two Cl atoms occupying the axial positions. Four $HPyC^-$ ligands provide four nitrogen atoms to occupy the equatorial plane of the Cu atom and further connect it with four Th_6 clusters (Fig. 2c). The two kinds of metal/cluster nodes are connected together by a series of ligands to form a 3D framework containing 1D open channels along the c axis (Fig. 2e). Structure simplification and calculation show that the topological type of compound **2** is a (4,8)-connected ***scu*** net with Schläfli symbol of $(4^{16}{\cdot}6^{12})(4^4{\cdot}6^2)_2$ [41].

$(CuCl_2)_2Th_6(\mu_3\text{-}O)_4(\mu_3\text{-}OH)_4(HPyC)_{10}(HCOO)_2(H_2O)_6$ (**3**). As with compound **2**, compound **3** also crystallizes in the orthorhombic space group *Pbam* due to their similar asymmetric units and coordinate environments (Table S1 and Fig. S2a in Supporting information). In compound **3**, the Cu atom also adopts an elongated octahedral configuration defined by two Cl atoms at the axial positions and four N atoms of four $HPyC^-$ ligands in the equatorial plane (Figs. S2c and S3a in Supporting information). Although the Th_6 cluster of compound **3** is coordinated by ten

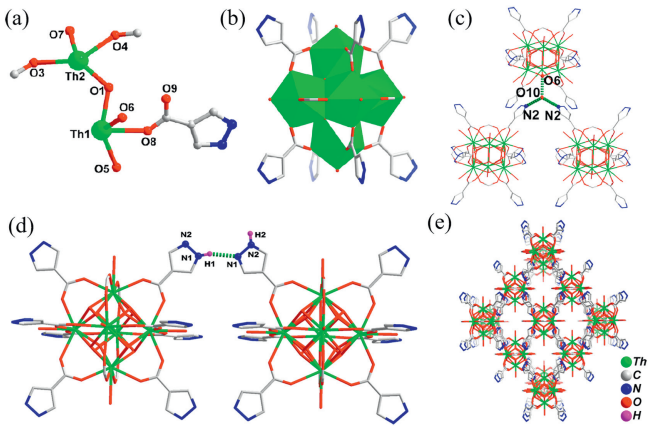

Fig. 1. (a) Asymmetric unit of compound **1**. (b) The structure of $Th_6(\mu_3\text{-}O)_4(\mu_3\text{-}OH)_4(H_2O)_6(HPyC)_8(HCOO)_4$ cluster. (c, d) Hydrogen bond interactions forces between adjacent Th_6 clusters. (e) 3D porous structure of compound **1** formed by hydrogen bonding. Color scheme: Th, green; Cu, cyan; C, gray; O, red; N, blue; H, pink. Most H atoms were omitted for clarity.

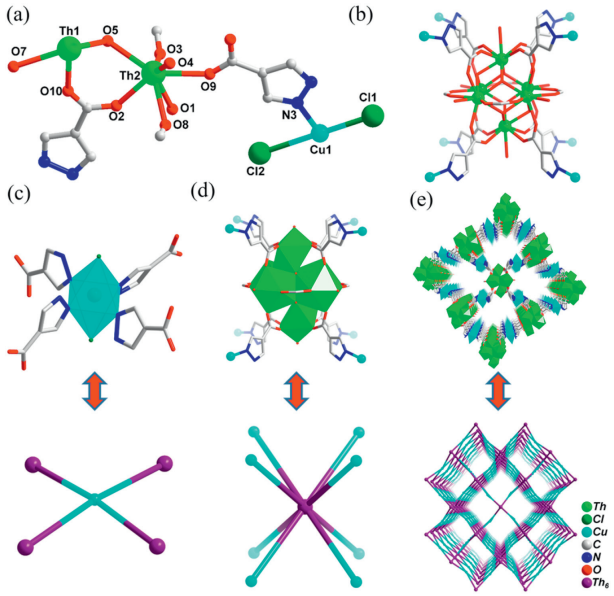

Fig. 2. (a) Asymmetric unit of compound **2**. (b) The $Th_6(HPyC)_8$ cluster connected with eight Cu atoms. (c) The Copper ion connected to four pyrazoles and viewed as a 4-connected node. (d) Th_6 cluster connected to eight copper ions and viewed as an 8-connected node. (e) 3D framework of compound **2** is classified as a (4,8)-connected ***scu*** net. Color scheme: Th, green; Cu, cyan; Cl, dark green; C, gray; O, red; N, blue; Th_6, purple. H atoms were omitted for clarity.

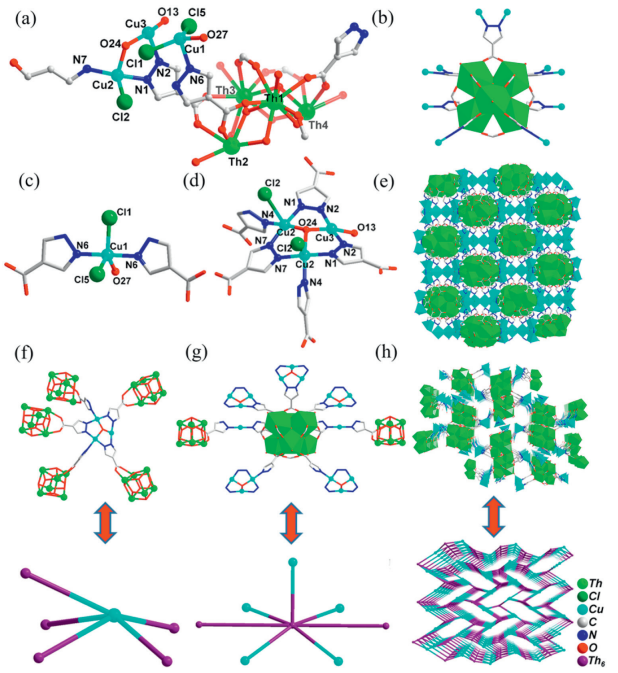

Fig. 3. (a) Asymmetric unit of compound **4**. (b) $Th_6(HPyC)_7$ cluster connected with ten Cu atoms. (c) The structure of trinuclear cluster $Cu_3(\mu_3\text{-}OH)(HPyC)_5$. (d) The coordination modes of Cu1 ion. (e) 3D framework of compound **4**. (f) Cu_3 cluster connected with five Th_6 clusters and viewed as a 5-connected node. (g) Th_6 cluster connected to five Cu_3 clusters and two Th_6 clusters and viewed as a 7-connected node. (h) The topology of compound **4** is classified as a (5,7)-connected net. Color scheme: Th, green; Cu, cyan; Cl, dark green; C, gray; O, red; N, blue; Th_6, purple. H atoms were omitted for clarity.

$HPyC^-$ ligands, only eight of which are further connected with Cu atoms and the other two ligands are free (Figs. S2b and S3c in Supporting information). Thus, the 3D framework of compound **3** is also classified as a (4,8)-connected ***scu*** net containing 1D open channels along the c axis (Figs. S2d and S3e). Due to the presence of $HPyC^-$ ligands that are not coordinated to Cu atoms in the 1D open channels, the solvent-accessible volume decreases from 58.6% of compound **2** to 53.7% of compound **3** calculated by PLATON routine [42].

$[Cu_3(\mu_3\text{-}OH)(H_2O)Cl_2][Cu(H_2O)Cl_2]Th_6(\mu_3\text{-}O)_4(\mu_3\text{-}OH)_4(PyC)_3(HPyC)_4(HCOO)_5(H_2O)_6$ (**4**). Compound **4** crystallizes in an orthorhombic space group *Pnma* (Table S1). The asymmetric unit of compound **4** contains four Th and three Cu atoms which are crystallographically independent, 3.5 $PyC^{2-}/HPyC^-$ ligands, 2.5 $HCOO^-$ ligands, three Cl^- anion and several coordinated $O^{2-}/OH^-/H_2O$ groups, as shown in Fig. 3a, Figs. S4a and b (Supporting information). In this unit, Th2 and Th4 are located at the special position of the symmetry axis with position occupancy of 0.5, whereas the occupancy of Th1 and Th3 is 1.0. Through an axisymmetric operation the whole $Th_6(\mu_3\text{-}O)_4(\mu_3\text{-}OH)_4$ cluster core of compound **4** is obtained, where seven edges are coordinated by the carboxylates from $PyC^{2-}/HPyC^-$ ligands, while the remaining five ones are coordinated by the carboxylates from $HCOO^-$ ligands (Figs. 3b and g). As shown in Fig. 3c, the Cu1 atom has a distorted triangular bipyramid configuration defined by two Cl atoms and one H_2O in the equatorial plane and two N atoms from two $HPyC^-$ ligands at the axial positions, respectively. Two Cu2 atoms and one Cu3 atom are bridged together by one μ_3-OH and three N_2 groups from three PyC^{2-} ligands to form a trinuclear cluster $Cu_3(\mu_3\text{-}OH)N_6$, in which Cu atoms adopt the square pyramidal or quadrilateral configurations, respectively (Figs. 3c and d). Therefore, the structure of compound **4** involves three kinds of metal nodes, hexanuclear cluster $Th_6(\mu_3\text{-}O)_4(\mu_3\text{-}OH)_4(COO)_{12}(H_2O)_6$, trinuclear cluster $Cu_3(\mu_3\text{-}OH)N_6$ and mononuclear $CuCl_2N_2(H_2O)$, which are bridged together through a series of $PyC^{2-}/HPyC^-$ ligands to construct a 3D framework, as shown in Fig. 3e. Topologically, Each Cu_3 cluster is connected with five Th_6 clusters and can be viewed as a 5-connected node (Fig. 3f). Each Th_6 cluster is connected with two Th_6 clusters and five Cu_3 clusters *via* two $Cu(HPyC)_2$ units and five $PyC^{2-}/HPyC^-$ ligands, respectively, and can be viewed as a 7-connected node (Fig. 3g). Structure simplification shows that the framework of compound **4** is classified as a (5,7)-connected net with Schläfli symbol of $(3^2.4^4.5^4)(3^4.4^6.5^6.6^5)$ calculated using the TOPOS program (Fig. 3h) [41]. Although tens of thousands of MOFs have been synthesized, there have been very few (5,7)-connected MOFs reported. To the best of our knowledge, this compound represents the first example of an An-MOF with (5,7)-connected net.

Compound **1** was formed by substitution of eight $HPyC^-$ ligands for the $HCOO^-$ ligands on the preassembled $Th_6O_4(OH)_4(H_2O)_6(HCOO)_{12}$ under solvothermal conditions, indicating that ligands on the Th_6 cluster are exchangeable. Meanwhile, the pyrazole N atom on $HPyC^-$ ligands has the coordination ability, and can further coordinate with heterometal atom to construct heterometallic ThCOFs. The introduced copper ions are used as the second metal node to connect four adjacent Th_6 cluster units *via* pyrazole nitrogen to form a ***scu***-type cubic net topology, in which eight of the $HCOO^-$ ligands of preassembled Th_6 cluster are also replaced by $HPyC^-$ ligands. However, the ligands $HPyC^-$ and formate on the Th_6 cluster are in a competitive coordination relationship, so eutectic compounds **2** and **3** with the same coordination and topologies were obtained, but with a different number of substituted $HPyC^-$ ligands on the Th_6 cluster, indicating the diversity of ligand substitution patterns. Further adjustment of the acidity of the reaction system by the addition of HCOOH affects the hydrolysis of copper ions to form a trinuclear copper cluster unit, which acts as a multi-coordination metal node to connect five Th_6 clusters to form compound **4** with a more complex (5,7)-connected net, in which seven of the $HCOO^-$ ligands of preassembled $Th_6O_4(OH)_4(H_2O)_6(HCOO)_{12}$ are replaced by $HPyC^-/PyC^{2-}$ ligands. The formation of new copper clusters causes significant structural changes and enhanced structural stability. However, the pre-assembled Th_6 cluster units are not affected by the system environment, and although the regulation reaction conditions may affect the number of exchanged ligands, the $Th_6O_4(OH)_4$ core structure remains stable. Therefore, it is feasible to construct cluster-based MOFs *via* ligand exchange strategy based on preassembled Th_6 cluster. In addition, the reversibility of ligand exchange also endows cluster-based MOFs with structural diversity.

The phase purity of compounds **1**–**4** can be confirmed through PXRD (Fig. S6 in Supporting information). The PXRD spectra of compounds **1** and **4** are consistent with the simulated results, indicating the high phase purity. Moreover, compound **4** exhibits excellent stability in water over a wide pH range. For compounds **2** and **3**, because they are eutectic compounds with similar coordination patterns and topologies, it is difficult to confirm their purity. Therefore, subsequent physicochemical characterization was carried out with compound **2** as the representative, and the discussion of the physicochemical properties of the relevant compounds is in Supporting information.

On the one hand, compound **4** exhibits excellent stability, on the other hand, Th_6 clusters and unsaturated trinucleated copper can provide Lewis acid and active sites for catalytic reactions [22]. Therefore, this porous heterometallic ThCOF is expected to be used for catalytic cycloaddition of epoxides. Initially, epichlorohydrin (1 mmol) was selected as the model substrate, and under a typical reaction condition, 9.3 mg (0.003 mmol, 0.3%) catalyst, 16.2 mg (0.05 mmol, 5 mol%) co-catalyst (tetrabutylammonium bro-

Table 1
Synthesis of various cyclic carbonates from CO_2 and epoxides.[a]

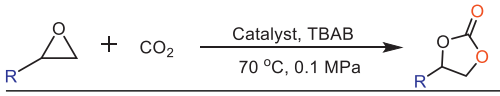

Entry	Epoxides	Products	Time (h)	Yield (%) [b]	TON [c]	TOF (h^{-1}) [d]
1			6	>99	333	55.5
2			6	>99	333	55.5
3		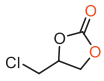	6	>99	333	55.5
4 5 6	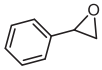	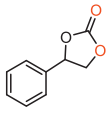	6 12 24	10 22 43	33 73 143	5.5 6.1 6.0
7 8 9	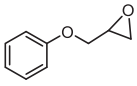	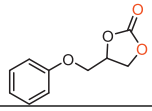	6 12 24	40 63 70	133 210 233	22.2 17.5 9.7

[a] Reaction conditions: epoxide (1 mmol), CO_2 (0.1 MPa), 70 °C, catalyst/TBAB (0.3/5 mol%).
[b] Total yield determined by ^1H NMR.
[c] TON: moles of cyclic carbonate per mole of catalyst used.
[d] TOF: moles of cyclic carbonate per mole of catalyst used per hour.

mide (TBAB)), 1 mL acetonitrile, 0.1 MPa CO_2, and 70 °C reacted for 12 h. The corresponding cyclic carbonate yield can exceed 99% (entry 1, Table S3 and Figs. S11-S15 in Supporting information). Subsequently, further exploration was conducted on the influence of reaction conditions on catalytic efficiency. The catalytic efficiency was found to hardly change when the reaction time or cocatalyst dosage was reduced by half. Even if the catalyst, cocatalyst and reaction time are reduced at the same time, the reaction efficiency can still reach about 77%. In particular, the catalytic efficiency can reach 99% with 0.3 mol% catalyst and 5 mol% TBAB for 6 h, which can be used as a typical reaction condition for further experiments.

To further explore the catalytic performance of compound **4**, more cycloaddition reactions were carried out under typical conditions to explore the substrate scope. As shown in Table 1 (Figs. S16-S23 in Supporting information), for alkyl epoxy substrates with smaller molecular sizes, such as 1,2-oxanephthenane and 1,2-epoxybutene, the catalytic efficiency can exceed 99%. While for epoxides containing benzene rings, such as epoxy styrene and glycerol phenyl ether, the catalytic efficiency is only about 10% and 40%, respectively. We further studied the influence of reaction time on its catalytic efficiency. With the extension of reaction time (24 h), the catalytic efficiency increased significantly (43% and 70%, respectively). The reason for the huge difference in catalytic efficiency should be due to the steric hindrance effect of the substituents. The 1D channel structure of compound **4** can be divided into two irregular small pores by the chloride ions coordinated on the Cu_3 cluster, where the maximum size is about 6 Å (Fig. S5 in Supporting information). We further calculated the size of different epoxy substrate molecules and found that alkyl epoxides can easily enter the pores, while epoxy compounds with benzene rings are difficult to enter and diffuse [43]. In addition, after three consecutive catalytic cycles, no significant decrease was found in the catalytic activity of compound **4** (Fig. S24 in Supporting information), and the PXRD spectrum analysis of compound **4** before and after the reaction showed excellent stability of the catalyst (Fig. S7 in Supporting information).

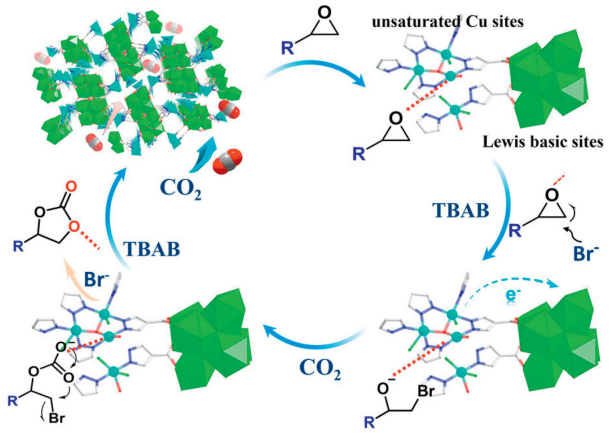

Fig. 4. Proposed catalytic mechanism for cycloaddition of epoxides and CO_2 to cyclic carbonate by compound **4**.

Combined with the structural characteristics of catalysts and literature reports, the possible mechanism of cycloaddition reaction is proposed [44,45], as shown in Fig. 4. Epoxides and CO_2 molecules are first attracted and enriched into the pore structure by hydrogen bonding and weak interactions. The oxygen atoms on the epoxide are then activated by forming coordination bonds with the unsaturated metal site copper ions, thereby weakening the C–O bonds in epoxides. Then, the nucleophilic Br^- anion of the cocatalyst TBAB attacks the carbon atoms with small steric hindrance on the epoxy ring, thereby opening the epoxy ring to form intermediate oxygen anions. Simultaneously, Th_6 clusters can provide Lewis acidic and defect sites for catalytic reactions and facilitate the transfer of electrons [27,46–48]. Polarized CO_2 rapidly combines with oxygen anions to form five-membered cyclic carbonate anions. Finally, Br^- is removed from the alky-carbonate anions, and the cocatalyst TBAB is released to complete the cyclization process.

From this catalytic process, the heterometallic unsaturated metal site copper cation and the Lewis basic site Th_6 cluster synergistically drive the catalytic reaction.

In summary, we have obtained three novel thorium cluster-based MOFs *via* the ligand exchange strategy. When copper ions are introduced to coordinate with the pyrazole-nitrogen end of the N/O bifunctional hybrid ligand H_2PyC, two kinds of thorium-copper heterometallic cluster organic frameworks with different topologies were obtained. Compounds **2** and **3** have similar coordination structures and the same ***scu***-type topological framework. The only difference is that in compound **3**, there are two additional $HPyC^-$ ligands on the equatorial plane of the Th_6 cluster, which do not further coordinate with copper ions. By adjusting the acidity of the system, the hydrolysis behavior of copper ion is further controlled. In compound **4**, trinuclear copper appears and serves as the metal node, forming a novel (5,7)-connected framework structure, which is first time reported in actinide-based MOFs. This new heterometallic ThCOF exhibits excellent stability and can be used as an effective catalyst for the cycloaddition of carbon dioxide with epoxides to form the corresponding cyclic carbonates. The ligand exchange strategy based on preassembled Th_6 cluster provides the possibility to controllable construct novel cluster-based MOFs materials. This work provides a valuable reference for the development and utilization of actinide heterometallic functional materials.

Declaration of competing interest

The authors declare that they have no known competing financial interests or personal relationships that could have appeared to influence the work reported in this paper.

Acknowledgments

We acknowledge the support of the National Natural Science Foundation of China (Nos. 22076187, 22122609), the Hunan Province Natural Science Foundation of China (No. 2023JJ40530), and the Scientific Research Fund of Hunan Provincial Education Department (No. 22C0202). We thank The National Science Fund for Distinguished Young Scholars (No. 21925603).

Supplementary materials

Supplementary material associated with this article can be found, in the online version, at doi:10.1016/j.cclet.2024.109642.

References

[1] V.K. Manchanda, Radiochim. Acta 111 (2023) 243–263.
[2] P. Yang, Z. Lin, W. Wan, et al., Int. J. Energy Res. 45 (2021) 12059–12070.
[3] K. Furukawa, L.B. Erbay, A. Aykol, Energy Conv. Manag. 63 (2012) 51–54.
[4] M.S. Kazimi, Am. Sci. 91 (2003) 408–415.
[5] Y. Liang, L. Mei, Q. Jin, et al., Chin. Chem. Lett. 33 (2022) 3539–3542.
[6] X. Zhang, L. Zhang, T. Bo, et al., Chin. Chem. Lett. 33 (2022) 3527–3530.
[7] J. Lu, K. He, Y. Wang, et al., Chin. Chem. Lett. 33 (2022) 3422–3428.
[8] S.M. McLennan, W.B. Nance, S.R. Taylor, Geochim. Cosmochim. Ac. 44 (1980) 1833–1839.
[9] K. Lv, S. Fichter, M. Gu, et al., Coord. Chem. Rev. 446 (2021) 1–81.
[10] Z.W. Huang, K.Q. Hu, X.B. Li, et al., J. Am. Chem. Soc. 145 (2023) 18148–18159.
[11] A.M. Hastings, D. Ray, S.L. Hanna, et al., Inorg. Chem. 61 (2022) 9480–9492.
[12] Y.B. Wu, C. Xiong, Q.Y. Liu, et al., Inorg. Chem. 60 (2021) 6472–6479.
[13] D. Meng, H. Liang, Q. Chen, et al., Chin. Chem. Lett. 29 (2018) 447–450.
[14] K.E. Knope, L. Soderholm, Chem. Rev. 113 (2013) 944–994.
[15] P. Li, X. Wang, K.I. Otake, et al., ACS Appl. Nano Mater. 2 (2019) 2260–2265.
[16] X.H. Kong, Q.Y. Wu, L. Mei, et al., CCS Chem. 5 (2023) 1144–1153.
[17] Z.J. Li, S. Guo, H. Lu, et al., Inorg. Chem. Front. 7 (2020) 260–269.
[18] Y. Wang, W. Liu, Z. Bai, et al., Angew. Chem. Int. Ed. 57 (2018) 5783–5787.
[19] Z. Xu, X. Xiong, J. Xiong, et al., Nat. Commun. 11 (2020) 3163.
[20] X. Kong, K. Hu, Z. Huang, et al., Inorg. Chem. 60 (2021) 14535–14539.
[21] Z.W. Huang, K.Q. Hu, L. Mei, et al., Dalton Trans. 49 (2020) 983–987.
[22] H. Xu, C.S. Cao, H.S. Hu, et al., Angew. Chem. Int. Ed. 58 (2019) 6022–6027.
[23] H. Lu, J. Xie, X.Y. Wang, et al., Nat. Commun. 12 (2021) 2798.
[24] J. Andreo, E. Priola, G. Alberto, et al., J. Am. Chem. Soc. 140 (2018) 14144–14149.
[25] H. Lu, H. Hou, Y.C. Hou, et al., J. Am. Chem. Soc. 144 (2022) 3449–3457.
[26] S.E. Gilson, M. Fairley, P. Julien, et al., J. Am. Chem. Soc. 142 (2020) 13299–13304.
[27] Q. Niu, Q. Huang, T.Y. Yu, et al., J. Am. Chem. Soc. 144 (2022) 18586–18594.
[28] C. Falaise, J.S. Charles, C. Volkringer, et al., Inorg. Chem. 54 (2015) 2235–2242.
[29] Y. Bai, Y. Dou, L.H. Xie, et al., Chem. Soc. Rev. 45 (2016) 2327–2367.
[30] Z. Chen, S.L. Hanna, L.R. Redfern, et al., Coord. Chem. Rev. 386 (2019) 32–49.
[31] H. Lu, M. Xu, Z. Zheng, et al., Inorg. Chem. 60 (2021) 18629–18633.
[32] Z.J. Li, Y. Ju, Z. Zhang, et al., Chem. Eur. J. 27 (2021) 17586–17594.
[33] Z.J. Li, Y. Ju, X.L. Wu, et al., Inorg. Chem. Front. 10 (2023) 1721–1730.
[34] Z. Zheng, H. Lu, X. Guo, et al., Chem. Commun. 57 (2021) 8131–8134.
[35] J. Lei, W. Yuan, J. Shang, et al., Inorg. Chem. 62 (2023) 15195–15205.
[36] W. Chen, Z. Wang, Q. Wang, et al., J. Am. Chem. Soc. 145 (2023) 4736–4775.
[37] Y. Chu, S. Xiong, Chin. Chem. Lett. 33 (2022) 486–490.
[38] M. Yin, R. Krishna, W. Wang, et al., CCS Chem. 4 (2022) 1016–1027.
[39] K.Q. Hu, Z.W. Huang, X.B. Li, et al., Adv. Funct. Mater. 33 (2023) 2213039.
[40] D. Juan, J.J. Good, V.H. DiStefano, et al., Eur. J. Inogr. Chem. 9 (2011) 1374–1377.
[41] V.A. Blatov, A.P. Shevchenko, D.M. Proserpio, Cryst. Growth Des. 14 (2014) 3576–3586.
[42] A.L. Spek, Acta Crystallogr. Sect. C: Struct. Chem. 71 (2015) 9–18.
[43] L. Wang, W. Qiao, H. Liu, et al., Inorg. Chem. 62 (2023) 3817–3826.
[44] X. Zhang, X. Wang, C. Li, et al., J. Colloid Interface Sci. 656 (2024) 127–136.
[45] X. Zhang, C. Li, T. Hu, ACS Sustain. Chem. Eng. 11 (2023) 17837–17848.
[46] J. He, J. Li, Q. Han, et al., ACS Appl. Mater. Interfaces 12 (2020) 2199–2206.
[47] S. Liu, H. Chen, X. Zhang, ACS Catal. 12 (2022) 10373–10383.
[48] J. Lyu, X. Zhang, P. Li, et al., Chem. Mat. 31 (2019) 4166–4172.